A noncanonical role of NOD-like receptor NLRP14 in PGCLC differentiation and spermatogenesis

Yike Yin[a], Shiyu Cao[a], Huancheng Fu[a], Xueying Fan[a], Jingfei Xiong[a], Qiuyue Huang[a], Yu Liu[b], Kun Xie[a], Tie-Gang Meng[c,d], Yuliang Liu[e], Dan Tang[f], Tingting Yang[g], Biao Dong[b], Shiqian Qi[f], Ling Nie[h], Huiyuan Zhang (张惠媛)[i], Hongbo Hu (胡洪波)[i], Wenming Xu[j], Fuping Li[g], Lunzhi Dai[b], Qing-Yuan Sun[c,k], and Zhonghan Li[a,l,1]

[a]Center for Growth Metabolism & Aging, Key Laboratory of Bio-Resource and Eco-Environment of Ministry of Education, College of Life Sciences, Sichuan University, 610064 Chengdu, China; [b]Department of General Practice and National Clinical Research Center for Geriatrics, State Key Laboratory of Biotherapy, West China Hospital, Sichuan University and Collaborative Innovation Center of Biotherapy, 610064 Chengdu, China; [c]State Key Laboratory of Stem Cell and Reproductive Biology, Institute of Zoology, Chinese Academy of Sciences, 100101 Beijing, China; [d]Fertility Preservation Lab, Reproductive Medicine Center, Guangdong Second Provincial General Hospital, 510317 Guangzhou, China; [e]Sichuan Key Laboratory of Conservation Biology for Endangered Wildlife, Chengdu Giant Panda Breeding Research Base, 610081 Chengdu, China; [f]Department of Urology, State Key Laboratory of Biotherapy, West China Hospital, Sichuan University and Collaborative Innovation Center of Biotherapy, 610064 Chengdu, China; [g]Human Sperm Bank, Key Laboratory of Birth Defects and Related Diseases of Women and Children of Ministry of Education, West China Second University Hospital of Sichuan University, 610064 Chengdu, China; [h]Department of Pathology, State Key Laboratory of Biotherapy, West China Hospital, Sichuan University and Collaborative Innovation Center of Biotherapy, 610064 Chengdu, China; [i]Department of Rheumatology and Immunology, State Key Laboratory of Biotherapy, West China Hospital, Sichuan University and Collaborative Innovation Center of Biotherapy, 610064 Chengdu, China; [j]Department of Obstetrics/Gynecology, Joint Laboratory of Reproductive Medicine, Key Laboratory of Obstetric, Gynecologic and Pediatric Diseases and Birth Defects of Ministry of Education, West China Second University Hospital, Sichuan University, 610064 Chengdu, China; [k]University of Chinese Academy of Sciences, 100000 Beijing, China; and [l]National Engineering Laboratory for Oral Regenerative Medicine, West China Hospital of Stomatology, Sichuan University, 610064 Chengdu, China

Edited by Vishva M. Dixit, Genentech, San Francisco, CA, and approved July 20, 2020 (received for review March 26, 2020)

NOD-like receptors (NLRs) are traditionally recognized as major inflammasome components. The role of NLRs in germ cell differentiation and reproduction is not known. Here, we identified the gonad-specific Nlrp14 as a pivotal regulator in primordial germ cell-like cell (PGCLC) differentiation in vitro. Physiologically, knock out of Nlrp14 resulted in reproductive failure in both female and male mice. In adult male mice, Nlrp14 knockout (KO) inhibited differentiation of spermatogonial stem cells (SSCs) and meiosis, resulting in trapped SSCs in early stages, severe oligozoospermia, and sperm abnormality. Mechanistically, NLRP14 promoted spermatogenesis by recruiting a chaperone cofactor, BAG2, to bind with HSPA2 and form the NLRP14–HSPA2–BAG2 complex, which strongly inhibited ChIP-mediated HSPA2 polyubiquitination and promoted its nuclear translocation. Finally, loss of HSPA2 protection and BAG2 recruitment by NLRP14 was confirmed in a human nonsense germline variant associated with male sterility. Together, our data highlight a unique proteasome-mediated, noncanonical function of NLRP14 in PGCLC differentiation and spermatogenesis, providing mechanistic insights of gonad-specific NLRs in mammalian germline development.

spermatogenesis | PGCLC differentiation | proteasome degradation | NLRP14

Pattern recognition receptors (PRRs) are the key surveillance components of mammalian innate immune responses, which sense the invading microbial molecules and trigger the downstream immune activation signaling cascade (1). While classical PRRs such as Toll-like receptors (TLRs) and C lectins are typically membrane associated, intracellular cytosolic PRR protein families were also discovered in recent years (2, 3). One such family is NOD-like receptors (NLRs), which recognize a variety of intracellular signals including microbial components, stress signals, and metabolites (4). Since the discovery, much attention has been paid to NLRs' roles in inflammasome assembly, innate and adaptive immune signaling, antiviral responses, and cell death (5, 6). However, other reports, such as transcriptional regulation of MHC class I by NLRC5 (7) and MHC class II by CIITA (8), suggested that the function of NLRs may be more diverse than initially thought. Physiological and tissue-specific functions of NLRs beyond inflammasomes remain to be identified.

Interestingly, several NLR members, such as Nlrp2 (9, 10), Nlrp5 (Mater) (11), and Nlrp7 (12), exhibited highly restricted expression in mammalian germline and acted as maternal effect genes. For example, both Nlrp2 and Nlrp5 were oocyte-specifically expressed and required for early embryonic development after fertilization (9–11). Nlrp7, without its ortholog in mice, was identified as a maternal gene, of which mutations were associated with hydatidiform moles and reproductive wastage in human patients (13). It is worth noting that, in the cases of Nlrp2 (10) and Nlrp5 (11), the phenotypes from knockout (KO) animals were clearly not immune-related, although the detailed mechanisms underneath these observations were not investigated. Nevertheless, these reports suggested that gonad-specific NLRs might act through a unique molecular mechanism beyond immune regulation, which is particularly interesting to us.

As an important member of the NLR family, Nlrp14 also has a gonad-specific expression pattern, mainly in the testis and secondarily in the ovary (ENCODE) (14). A recent report suggested

Significance

NOD-like receptors (NLRs) are traditionally recognized as key surveillance pattern recognition receptors (PRRs) during innate immune regulation. Several NLRs exhibit highly restricted expression in mammalian germline, where their physiological functions are largely unknown. Here we report that Nlrp14, an NLR specifically expressed in testis and ovary, plays a critical role in regulating germ cell differentiation and reproduction. Nlrp14 deficiency led to decreased primordial germ cell-like cell (PGCLC) differentiation in vitro and reproduction failure in both male and female mice in vivo. In the male mice, Nlrp14 knockout strongly compromised differentiation of spermatogonial stem cells and meiosis. Mechanistically, NLRP14 protected HSPA2 from proteasome-mediated degradation by recruiting BAG2, loss of which was further confirmed in a human mutation associated with male sterility.

Author contributions: Y.Y., H.Z., H.H., L.D., Q.-Y.S., and Z.L. designed research; Y.Y., S.C., H.F., X.F., J.X., Q.H., Yu Liu, K.X., T.-G.M, D.T., T.Y., and Z.L. performed research; H.F., Yuliang Liu, T.Y., L.N., W.X., F.L., and L.D. contributed new reagents/analytic tools; Y.Y., H.F., L.N., H.H., L.D., and Z.L. analyzed data; and Y.Y. and Z.L. wrote the paper.

The authors declare no competing interest.

This article is a PNAS Direct Submission.

[1]To whom correspondence may be addressed. Email: zhonghan.li@scu.edu.cn.

This article contains supporting information online at https://www.pnas.org/lookup/suppl/doi:10.1073/pnas.2005533117/-/DCSupplemental.

First published August 24, 2020.

that maternal Nlrp14 might function to suppress the nucleic acid-sensing pathway and was proposed to facilitate fertilization in human (15). However, Nlrp14 mutations were found to be associated with patients of spermatogenic failure rather than fertilization (16), suggesting that Nlrp14 might have a role in spermatogenesis instead. Nevertheless, no physiological study on Nlrp14 function was reported to date and the role of Nlrp14 in germ cell development remains unknown.

In this study, we identified Nlrp14 as a key regulator of primordial germ cell-like cell (PGCLC) differentiation from mouse embryonic stem cells (mESCs). Knockdown and KO of Nlrp14 both resulted in the substantial decrease in PGCLC differentiation. Physiologically, Nlrp14 KO led to reproduction failure in both female and male mice. In male mice, Nlrp14 deficiency resulted in severe sperm count decline and increased abnormality. Further investigation revealed that differentiation of spermatogonial stem cells (SSCs) and meiosis were strongly compromised in these KO animals, with increased expression and abnormal distribution of SSC markers at various stages and dramatic decrease of markers for mature spermatids. Mechanistically, immunoprecipitation (IP)-coupled mass spectrometry analysis discovered that mouse NLRP14 formed a complex with HSPA2, a testis-specific HSP70 family member that was required for germ cell differentiation and spermatogenesis (17). Further evidence suggested that NLRP14's binding with HSPA2 protected HSPA2 from ubiquitination-mediated proteasomal degradation, probably by recruiting the cochaperone factor BAG2 and promoted translocation of HSPA2 into the nucleus, where HSPA2 was required to facilitate spermatid DNA packaging (18, 19). Moreover, loss of HSPA2 protection and BAG2 recruitment by NLRP14 were also confirmed in a human nonsense germline variant associated with male sterility. Together, our data uncovered an intriguing proteasome-mediated noncanonical function of Nlrp14, which provides insights in understanding the function of gonad-specific NLRPs.

Results

Identification of Nlrp14 as a Key Regulator for PGCLC Differentiation. To discover potential candidate genes that may be important for germ cell specification and spermatogenesis, we first focused on genes with a testis-specific expression profile. Transcriptome datasets from ENCODE (14) including 24 tissues and 236 samples from 8-wk-old mice were analyzed; 1,584 genes with testis-specific expression were identified (Fig. 1*A*) and then cross-compared with differential expressed ones during PGCLC differentiation (from naïve mESCs to EpiLCs and finally PGCLCs), by reanalyzing data from the Gene Expression Omnibus (accession no. GSE30056) (20). Among the 25 genes identified by the cross-comparison, 10 were significantly induced in EpiLCs and/or PGCLCs during differentiation, and thus chosen as candidates for downstream validation (Fig. 1 *B* and *C*).

To investigate candidates' function in PGCLC differentiation, the same differentiation procedure was adopted as previously reported (*SI Appendix*, Fig. S1*A*) (20), and the morphology and correct sequential induction of EpiLC and PGCLC markers were confirmed (*SI Appendix*, Fig. S1 *B* and *C*). Three short hairpin RNAs (shRNAs) were designed for each candidate gene and cloned into pLKO.1 lentiviral vector. The shRNA lentivirus was pooled together before transduction. Transduced mESCs (AB2.2) were then induced for PGCLC differentiation. STELLA immunostaining (anti-DPPA3) was used to evaluate PGCLC differentiation efficiency (*SI Appendix*, Fig. S1*D*). Among the 10 candidate genes tested in our assay, knockdown of Nlrp14 exhibited strongly decreased STELLA immunostaining (*SI Appendix*, Fig. S1*E*), suggesting its potential role to regulate PGCLC differentiation.

Nlrp14 Was a Potent Regulator of PGCLC Differentiation In Vitro. According to the data from ENCODE (14), mouse Nlrp14 had a highly specific expression profile and was found only in testis and ovary with two transcripts, which were also confirmed in our experiments (*SI Appendix*, Fig. S2 *A–D*). More importantly, Nlrp14 was highly induced in EpiLCs and PGCLCs during differentiation (*SI Appendix*, Fig. S2*E*).

To investigate whether Nlrp14 was indeed a potent regulator of PGCLCs, three shRNAs were individually transduced into mESCs before inducing PGCLC differentiation. Nlrp14 was efficiently knocked down by all three shRNAs (Fig. 1*D*), while the overall morphology and growth of EpiLCs and PGCLC spheres were not affected (Fig. 1*E* and *SI Appendix*, Fig. S2 *F* and *G*). Quantitative analysis for EpiLCs and PGCLCs marker expression indicated that Nlrp14 knockdown resulted in significantly decreased expression of PGCLC (Fig. 1*F*) but not EpiLC markers (Fig. 1*G*). STELLA immunostaining also indicated a substantial decrease of STELLA-positive cells in Nlrp14 knockdown spheres (Fig. 1*H*). To further confirm our findings from shRNA experiments, an Nlrp14 KO mESC line was generated using CRISPR-Cas9 and confirmed by sequencing (*SI Appendix*, Fig. S3 *A–C*). The pluripotency of Nlrp14 KO mESCs was verified by Nanog, Oct4, and Sox2 immunostaining (*SI Appendix*, Fig. S3*D*). When Nlrp14 KO mESCs were induced to form PGCLC spheres, similar phenotype as RNA interference (RNAi) experiments were observed. The overall morphology of EpiLCs and PGCLC spheres was not affected (*SI Appendix*, Fig. S3 *E* and *F*), while STELLA-positive cells were substantially decreased in PGCLC spheres (*SI Appendix*, Fig. S3*G*). RT-qPCR analysis of EpiLC and PGCLC markers again supported that Nlrp14 KO would significantly inhibit PGCLC differentiation (*SI Appendix*, Fig. S3 *H* and *I*). Together, these data suggested that Nlrp14 was a critical regulator of PGCLC differentiation in vitro.

Nlrp14 KO Strongly Inhibited Spermatogenesis in Mice. To investigate the physiological function of Nlrp14, KO mice were generated by the CRISPR-Cas9 method, and two lines with frameshift mutations in the Nlrp14 coding sequence were acquired (*SI Appendix*, Fig. S4 *A* and *B*). Nlrp14 KO animals exhibited no obvious developmental defects (*SI Appendix*, Fig. S4*C*) and had normal Mendelian distribution in birth (*SI Appendix*, Fig. S4*D*). However, both female and male KO animals exhibited serious reproduction failure during 10-wk continuous breeding, while heterozygous ones did not (Fig. 2*A*). While female KO mice exhibited to be 100% sterile, a few of the male ones did manage to sire offspring pups, which indicated that male reproductivity was not completely prohibited. Our initial assessment found that sections of the developing ovary appeared to be normal in female mice (*SI Appendix*, Fig. S4*E*); therefore, we decided to focus our work on the male spermatogenesis process in this study.

While no difference was observed for overall appearance and gonad-somatic index among testis from wild-type (WT), heterozygous, and KO mice (*SI Appendix*, Fig. S4*F*), hematoxylin/eosin (H&E) staining did reveal a substantial decrease of mature spermatozoa in seminiferous tubules (Fig. 2*B*), increased apoptosis (Fig. 2 *C* and *D*), and increased expression and cleavage of caspase proteins (*SI Appendix*, Fig. S4 *G* and *H*) in KO mice. In addition, both sperm count and motility were significantly declined in samples from cauda epididymis of KO mice (Fig. 2 *E–G* and Movies S1–S3). However, when the sperms were stimulated under human tubal fluid condition, which was normally used for mouse and human in vitro fertilization (21, 22), their motility could be mostly restored (*SI Appendix*, Fig. S4 *I* and *J*). Moreover, a substantially higher percentage of abnormal sperms was also noticed in KO animals as revealed by scanning electron microscopy analysis, such as proximal/distal bent tail, cytoplasmic retention, headless, amorphous head, etc. (Fig. 2 *H* and *I*). Together, these data suggested that Nlrp14 KO resulted in seriously compromised spermatogenesis and infertility in KO animals.

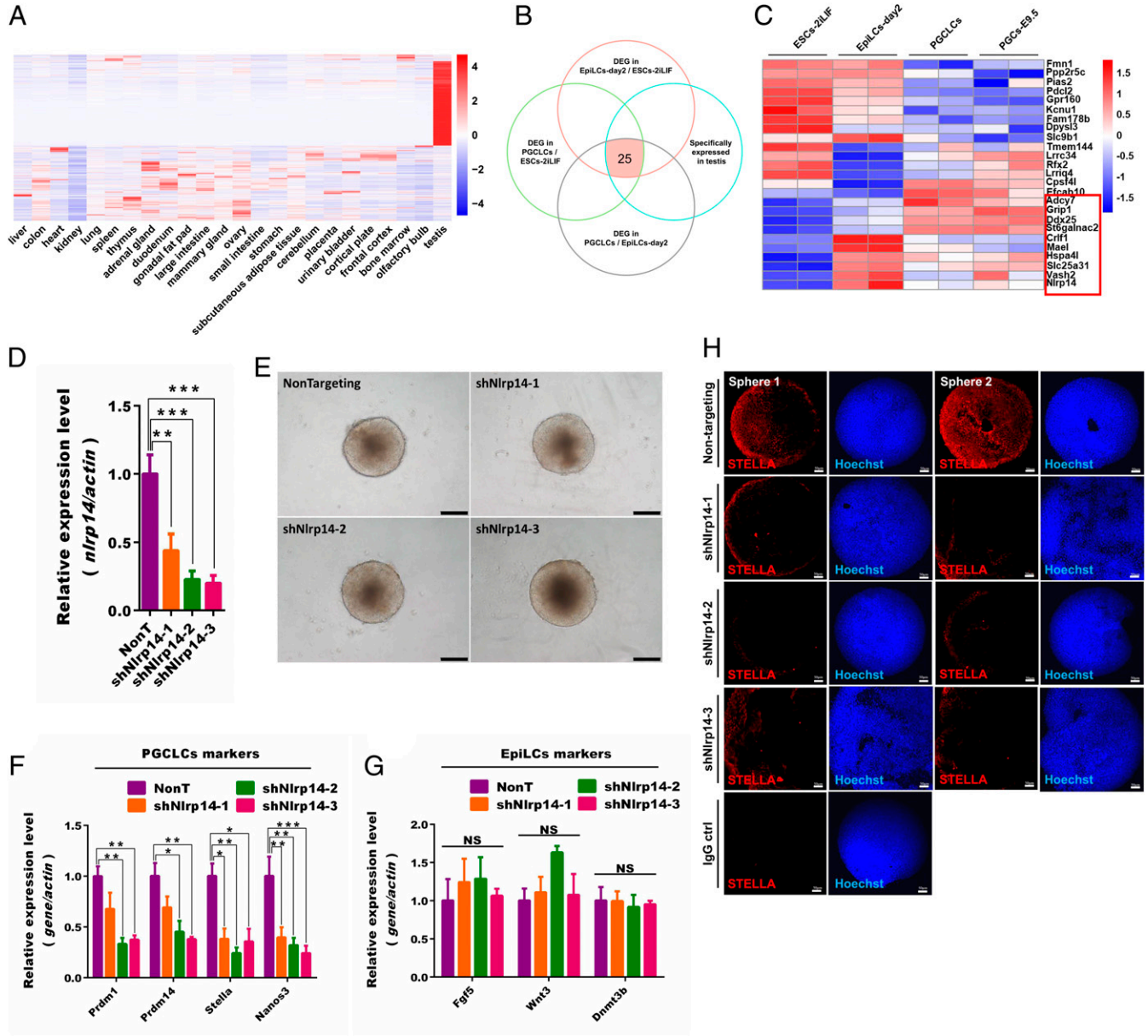

Fig. 1. Identification of Nlrp14 as a key regulator of PGCLC differentiation. (*A*) Heatmap of genes specifically expressed in mouse testis. RNA-seq datasets of 24 tissues from ENCODE were reanalyzed; 1,584 genes were testis specific. (*B*) The 25 genes with differential expression during PGCLC differentiation were identified as potential candidates. Venn diagram of genes differentially expressed in testis, mESCs in 2i+LIF medium, day2 EpiLCs, and PGCLCs are shown. (*C*) Ten candidate genes induced either in EpiLCs or PGCLC sphere were chosen for the downstream shRNA screen. Heatmap of 25 genes' differential expression among testis, mESCs in 2i+LIF medium, day2 EpiLCs, and PGCLCs is shown. The red outlined box shows the genes enriched in EpiLCs and/or PGCLCs. (*D*) The knockdown of Nlrp14 was confirmed in PGCLC spheres by RT-qPCR. Error bar represent data from three independent experiments. Nontargeting shRNA was used as the negative control. Data were normalized to actin expression. Statistics were calculated using SPSS software (one-way ANOVA followed by Tukey post hoc multiple comparisons). $^{**}P < 0.01$, $^{***}P < 0.001$. (*E*) The knockdown of Nlrp14 had minimal impact on the overall appearance of PGCLC spheres. Representative images of PGCLCs spheres from each shNlrp14 group are shown. (Scale bar: 200 μm.) (*F*) The expression of PGCLCs markers was significantly decreased in shNlrp14 spheres. Total RNAs were extracted using the TRIzol method. Expression of Prdm1, Prdm14, Stella, and Nanos3 was analyzed by RT-qPCR. Nontargeting shRNA was used as the negative control. Error bar represents data from three independent experiments. Statistics were calculated using SPSS software (one-way ANOVA followed by Tukey post hoc multiple comparisons). $^{*}P < 0.05$, $^{**}P < 0.01$, $^{***}P < 0.001$. (*G*) The expression of EpiLCs markers was not affected by Nlrp14 knockdown. Fgf5, Wnt3, and Dnmt3b were used as EpiLCs markers. Error bar represents data from three independent experiments. Statistical analysis is the same as in *F*. NS, not significant. (*H*) The knockdown of Nlrp14 resulted in severely decreased expression of STELLA in PGCLC spheres. The shRNA-transduced PGCLC spheres were immunostained with anti-STELLA antibody and imaged under the same exposure time. Hoechst was used for nuclear staining. (Scale bar: 50 μm.)

Nlrp14 KO Disrupted Differentiation of Spermatogonial Stem Cell and Meiosis. To further elucidate which stages were affected by Nlrp14 KO during spermatogenesis, marker genes representing different spermatogenic states were analyzed by immunohistofluorescence (IHF) and immunohistochemistry (IHC) (Fig. 3*A*). The specificity of each antibody was individually validated before use (*SI Appendix*, Fig. S5). Among these markers, DDX4 is exclusively expressed in PGCs just after they colonize embryonic gonads and in germ cells undergoing the gametogenic process until the postmeiotic stage (23). Cyclin D2 is expressed in

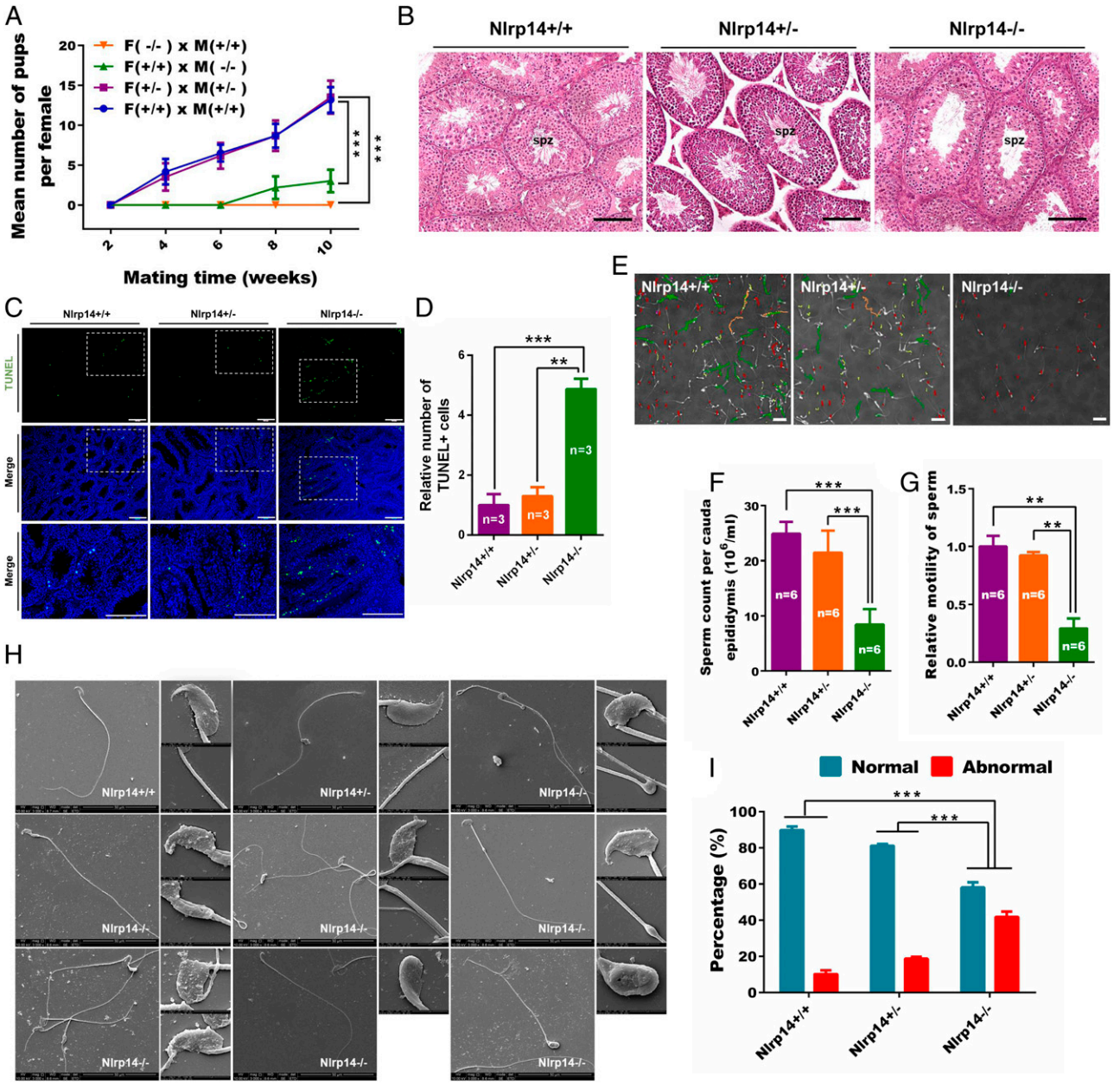

Fig. 2. Targeted disruption of Nlrp14 caused infertility and abnormal spermatogenesis in mice. (*A*) Nlrp14 KO mice exhibited strongly compromised fertility. Female mice were completely sterile, while male reproduction was severely compromised. Adult KO, heterozygous, and WT mice were set up for 10 wk of continuous breeding (six pairs for each experimental group). The reproductive ability of each WT mice was confirmed before breeding with KO ones. Age of mice: 3 mo. Error bar represents data from six breeding pairs. Statistics: one-way ANOVA followed by Tukey post hoc multiple comparisons. ***$P < 0.001$. (*B*) H&E staining revealed a decreased number of spermatozoa in Nlrp14 KO mice compared with WT and heterozygous littermates. Representative images of each genotype are shown; spz, spermatozoa. (Scale bar: 100 μm.) (*C*) The increase of apoptosis was identified in sections from the Nlrp14 KO testis. Three testes from each genotype were analyzed by terminal deoxynucleotidyl transferase dUTP nick end labeling (TUNEL) assay and representative images were shown. The dashed boxes show the zoomed-in area. (Scale bar: 200 μm.) (*D*) Quantitative analysis of TUNEL signals also confirmed the increase of cell apoptosis in Nlrp14 KO testis. The relative number of TUNEL+ cells was measured by the count of TUNEL signal per section of each genotype and normalized to $Nlrp14^{+/+}$ animals using the ImageJ software. Error bar represents data from two sections from three mice of each genotype. Statistics: one-way ANOVA followed by Tukey post hoc multiple comparisons (by SPSS). ***$P < 0.001$, **$P < 0.01$. (*E*) Both sperm quantity and motility were significantly decreased in Nlrp14 KO mice. The quantity and motility of sperms within cauda epididymis of each genotype were measured by computer-assisted sperm analysis (CASA). (Scale bar: 50 μm.) (*F*) A decrease in sperm count was detected in Nlrp14 KO mice. The concentration of sperms in cauda epididymis of each genotype were quantified. Sperms were released from cauda epididymis in 37 °C phosphate-buffered saline, and the sperm number was quantified using a hemocytometer. Error bar represents data from six mice of each genotype (counted three times for each sample). Statistics: one-way ANOVA followed by Tukey post hoc multiple comparisons (by SPSS). ***$P < 0.001$. (*G*) Sperm motility dropped significantly in Nlrp14 KO mice. Error bar represents data from six mice of each genotype. Motility was measured by CASA. Statistics: one-way ANOVA followed by Tukey post hoc multiple comparisons (by SPSS). **$P < 0.01$. (*H*) Representative images of sperms with various abnormalities in Nlrp14 KO mice. Samples were analyzed using an electron microscope, and representative abnormal sperms in Nlrp14 KO mice are shown. Images of WT sperm were used as the reference. (Scale bar: 50 μm in larger images, 5 μm in smaller ones.) (*I*) A significant increase in abnormal sperms was observed in Nlrp14 KO mice. Sperms were released from cauda epididymis, and, after staining with hematoxylin, the total number of normal and abnormal was counted under the microscope. For each mouse (sample), six random view fields were assessed and quantified (~1,600 sperms, in total). Error bar represents data from six mice of each genotype. Statistics: the χ^2 test (by SPSS). ***$P < 0.001$.

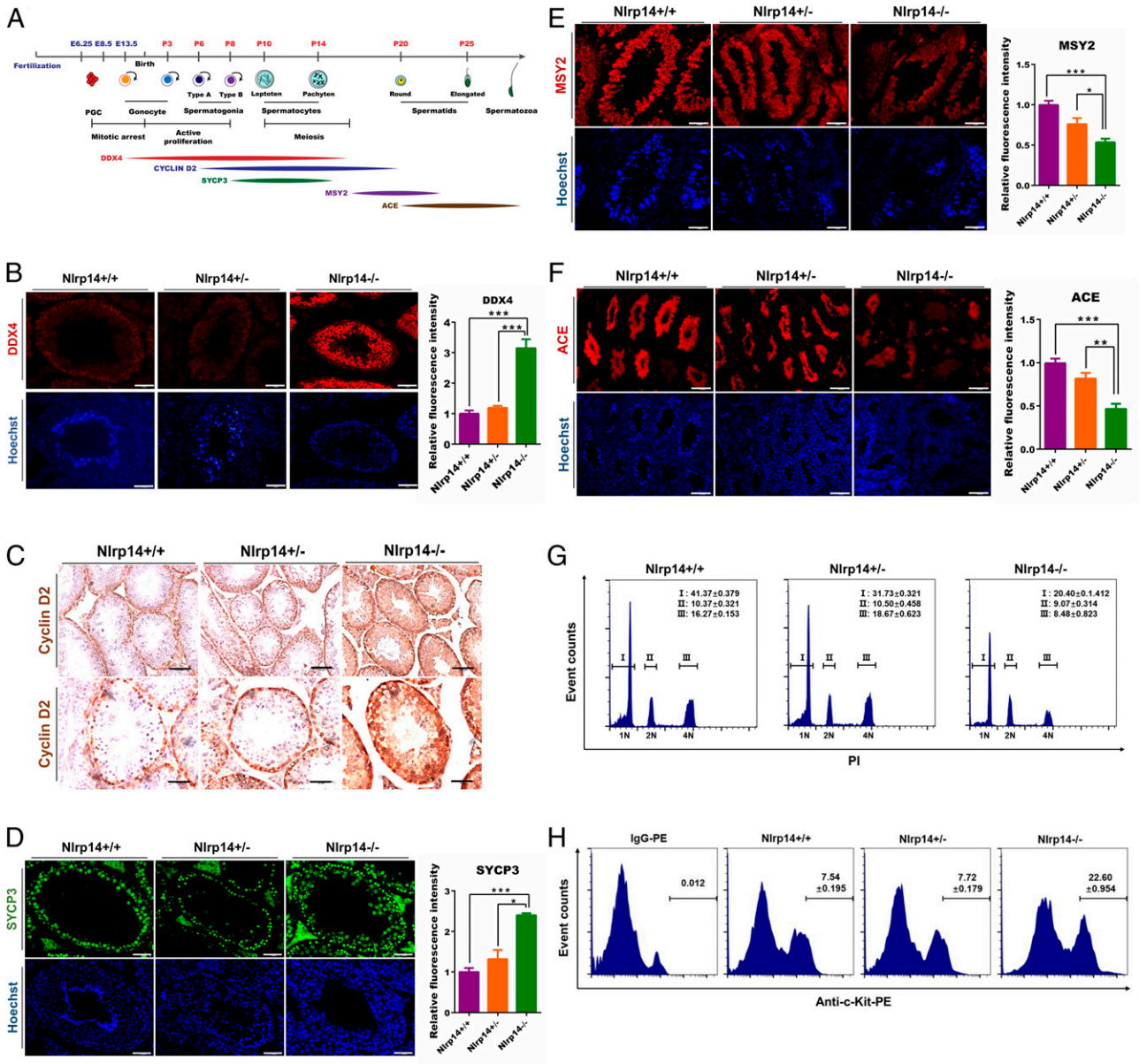

Fig. 3. Differentiation of SSCs and meiosis was compromised in Nlrp14 KO mice. (*A*) Schematic of the timeline and marker expression during male germ cell development in mice. Representative markers of different developmental stages were chosen for immunostaining analysis. (*B*) DDX4 (red) expression level was increased in the Nlrp14 KO testis. Abnormal DDX4-expressing cells were observed near the central region of seminiferous tubules. Testis sections of each genotype were immunostained with an anti-DDX4 antibody. Images were taken under the same exposure time. The relative fluorescence intensity was measured by quantification of fluorescence signal per area and normalized to WT animals using the ImageJ software. Error bar represents data from four to five random seminiferous tubules of two mice for each genotype. Statistics: one-way ANOVA followed by Tukey post hoc multiple comparisons (by SPSS). ***$P < 0.001$. (Scale bar: 50 μm.) Age of mice: 2 mo. (*C*) An increase of Cyclin D2 (brown) expression and abnormal distribution in testicular tubules were detected in KO animals. (Scale bar: 100 μm [*Upper*]; 50 μm [*Lower*].) Age of mice: 2 mo. (*D*) The expression and localization of SYCP3 (green) were also significantly changed in the Nlrp14 KO testis. Increased expression of SYCP3 was detected, and its localization in testicular cells showed abnormal enrichment toward the center of testicle tubules. Relative fluorescence intensity was measured the same as in *B*. Error bar represents data from four to five random seminiferous tubules of two mice for each genotype. Statistics: one-way ANOVA followed by Tukey post hoc multiple comparisons (by SPSS). *$P < 0.05$, ***$P < 0.001$. (Scale bar: 50 μm.) Age of mice: 2 mo. (*E*) MSY2 (red) expression level was decreased in the Nlrp14 KO testis. Relative fluorescence intensity was measured the same as in *B*. Error bar represents data from four to five random seminiferous tubules of two mice for each genotype. Statistics: one-way ANOVA followed by Tukey post hoc multiple comparisons (by SPSS). *$P < 0.05$, ***$P < 0.001$. (Scale bar: 50 μm.) Age of mice: 2 mo. (*F*) The ACE (red) expression level was also decreased in the Nlrp14 KO testis. Relative fluorescence intensity was measured the same as in *B*. Error bar represents data from four to five random seminiferous tubules of two mice for each genotype. Statistics: one-way ANOVA followed by Tukey post hoc multiple comparisons (by SPSS). **$P < 0.01$, ***$P < 0.001$. (Scale bar: 50 μm.) Age of mice: 2 mo. (*G*) DNA content analysis also revealed disrupted spermatogenesis in Nlrp14 KO mice. Testis samples from two adult animals of each genotype were pooled and analyzed by fluorescence-activated cell sorter (FACS). The representative FACS profile of each genotype was showed. Propidium iodide (PI) was used for DNA content staining. Cells with sub-1N DNA content represent spermatozoa with condensed chromatin. Cells with sub-2N DNA content represent spermatogonia and pre-meiotic spermatogonia. When the premeiotic spermatogonia were replicated, their DNA content would become 4N. The percentage of each cell group with different DNA content after removed cell debris and adhesions is shown. The "±" represents data from three replicates of the pooled samples;10,000 total events were collected and analyzed for each sample. Data were processed by FlowJo. (*H*) The c-Kit$^+$ germ cells were increased in Nlrp14 KO mice. Testes from two adult animals of each genotype were pooled and processed. Representative FACS profile of each genotype testis is shown. IgG-PE was used as the negative control. The "±" represent data from three replicates of the pooled samples; 10,000 total events were collected and analyzed for each sample. Data were analyzed by FlowJo.

spermatogonia when A_{a1} spermatogonia differentiate into A_1 one, and in spermatocytes and spermatids (24). Sycp3 first appears in leptotene spermatocytes and disappears in late meiotic cells (25). Msy2 is highly expressed in postmeiotic round spermatids (26), and Ace is expressed only in postmeiotic spermatogenic cells and sperm (27). IHF and IHC analysis indicated that DDX4 and Cyclin D2 expression were increased in testis sections from Nlrp14 KO mice (Fig. 3 *B* and *C* and *SI Appendix*, Fig. S6*A*). The distribution of DDX4 and Cyclin D2 signal was also shifted toward the center of the seminiferous tubules (Fig. 3 *B* and *C*). A similar phenotype was noticed in SYCP3 IHF analysis as well (Fig. 3*D* and *SI Appendix*, Fig. S6*B*). These data suggested that the differentiation of SSCs was significantly disrupted, and expression of stem cell markers was not turned off properly. On the other hand, the postmeiotic markers MSY2 and ACE were substantially decreased in KO animals (Fig. 3 *E* and *F* and *SI Appendix*, Fig. S6*C*), indicating that the meiotic process was interrupted. To exclude the potential contribution of Sertoli cells in these phenotypes, Sox9, a well-documented marker for Sertoli cells (28), was analyzed by IHF, and no significant change of $Sox9^+$ Sertoli cells was noted among WT, heterozygous, and KO animals (*SI Appendix*, Fig. S6 *D* and *E*). To further confirm these observations, DNA content and the percentage of c-Kit^+ germ cells were analyzed by flow cytometry. Decreased 1N and 4N populations and a spike of c-Kit+ germ cells were observed in Nlrp14 KO animals (Fig. 3 *G* and *H*). Together, these data suggested that Nlrp14 KO strongly compromised normal differentiation of SSCs and meiosis, and trapped many of the stem cells in an undifferentiated state, which, in turn, caused substantially decreased and abnormal spermatogenesis and infertility in KO animals.

NLRP14 Regulated Spermatogenesis through Interacting with HSPA2. To investigate the molecular mechanism for NLRP14-mediated regulation of spermatogenesis, we decided to employ a relatively unbiased approach by IP-coupled mass spectrometry analysis to identify potential NLRP14 interacting proteins. C18-4 cells, an immortalized cell line from A_s SSCs (29), was chosen for Nlrp14 overexpression and IP. The identity of C18-4 cells was confirmed first by Oct4 immunostaining (*SI Appendix*, Fig. S7*A*) and RT-PCR analysis of Ddx4, Dazl, and Plzf (*SI Appendix*, Fig. S7*B*), which were characterized in the original report (29). Next, Flag-tagged Nlrp14 was cloned from mouse testis complementary DNA. As the control, a STOP codon mutation was introduced at the 138th amino acid (aa) (Fig. 4*A*) to mimic the truncated mutant that had been associated with male spermatogenesis failure in human (16) and maintain the vector size for cotransfection at the same time. IP and silver staining results indicated that several specific bands were enriched in WT NLRP14 sample but not in IgG control or mutant NLRP14 (Fig. 4*B*). Mass spectrometry analysis identified the two most abundant proteins from these bands, HSPA2 and HSP70. Indeed, HSPA2 and HSP70 were specifically pulled down by WT NLRP14 but not IgG or mutant NLRP14 (Fig. 4*C*). To further confirm the interaction, reverse IP using HSPA2 and HSP70 antibodies was also performed (Fig. 4*D* and *SI Appendix*, Fig. S7*C*). Domain mapping experiments indicated that NLRP14 might bind with HSPA2 and HSP70 through multiple domains (Fig. 4 *E* and *F*), while both HSPA2 and HSP70 interacted with NLRP14 mainly through their NBD domain (Fig. 4 *G* and *H* and *SI Appendix*, Fig. S7 *D* and *E*). For HSPA2, its NBD domain could interact with both NACHT and LRR domains of NLRP14 (Fig. 4*H*). Together, these data confirmed that NLRP14 indeed specifically interacted with HSPA2 and HSP70.

To further dissect which interaction might be associated with the phenotypes we observed in KO animals, we set out to test the functional consequence of HSPA2 and HSP70's interaction with NLRP14. Previous reports indicated that HSPA2 was closely involved in germ cell development and spermatogenesis (30). Meanwhile, HSPA2 seems to be highly regulated through proteasome-mediated degradation mechanisms during spermatogenesis (17, 31). From our results, NLRP14 overexpression indeed resulted in increased expression of HSPA2 in C18-4 (Fig. 4 *C* and *D*). Meanwhile, HSPA2 was significantly decreased in Nlrp14 KO testis but not in WT or heterozygous ones (Fig. 4*I*), while transcription of mRNAs remained similar (*SI Appendix*, Fig. S7*F*). These data suggested that NLRP14 might interfere with the protein degradation of HSPA2. Indeed, cotransfection of WT Nlrp14 with Hspa2 indicated that binding with NLRP14 protected HSPA2 from polyubiquitination-mediated degradation, but not with mutant Nlrp14 (Fig. 4*J*). In addition, when previously reported single-cell RNA sequencing (RNA-seq) data were reanalyzed (32), expression of Nlrp14 was found to be closely associated with Hspa2 across different stages of spermatogenesis, but not with Tbk1, Bag6, or Cdk1, which were all documented coding genes for NLRP14 or HSPA2 interacting proteins (Fig. 4*K*) (15, 31, 33). Together, these data supported that NLRP14 could specifically bind with HSPA2 and protected it from polyubiquitination-mediated degradation. It is also worth noting that cotransfection of Nlrp14 with Hsp70 did not affect the polyubiquitination of HSP70 (*SI Appendix*, Fig. S7*G*), while, on the other hand, ubiquitination of NLRP14 was decreased (*SI Appendix*, Fig. S7*H*), which was deemed to be reasonably expected for HSP70's chaperone activity. HSP70 expression was also decreased in KO animals, although to a lesser extent (*SI Appendix*, Fig. S7*I*). Therefore, the NLRP14/HSPA2 axis seemed to be the main functional complex that was involved in PGCLC differentiation and spermatogenesis.

NLRP14 Recruited BAG2 to Inhibit ChIP-Mediated Ubiquitination. To further dissect the molecular mechanism for NLRP14-mediated inhibition of HSPA2 ubiquitination, a full-spectrum mass spectrometry analysis on NLRP14-immunoprecipitated sample was performed in C18-4 cells (Fig. 5*A*). Seven proteins were significantly enriched in WT Nlrp14 sample compared with those of IgG control and mutant Nlrp14 (Fig. 5*B*). Among them, Bag2 (BCL2-associated athanogene 2) was previously reported as a cochaperone protein with potent ubiquitin ligase inhibitory activity (19, 34). Moreover, in MEFs, BAG2 was found to bind with HSPA2 and protected it from ChIP-mediated proteasomal degradation (35). To confirm that NLRP14, HSPA2, and BAG2 indeed formed a complex together, repeat IP and reverse IP were performed, which supported that NLRP14, BAG2, and HSPA2 could specifically interact with each other and that the three proteins were indeed contained in one complex (Fig. 5 *C*–*E*). IP analysis of endogenous proteins also confirmed the interaction between NLRP14, BAG2, and HSPA2, where NLRP14 enhanced BAG2's IP by endogenous HSPA2 (Fig. 5*F*). Moreover, together with NLRP14, BAG2 strongly inhibited the polyubiquitination of HSPA2 (Fig. 5*G*). Since carboxy-terminus of HSP70 interacting protein (ChIP) was one of the key E3 ligases which regulated a broad spectrum of HSP70s and their clients including HSPA2 (36), we also set out to test whether NLRP14 and BAG2 could inhibit ChIP-mediated HSPA2 ubiquitination process. Overexpression of ChIP resulted in strong polyubiquitination of HSPA2 (Fig. 5*H*). Notably, neither NLRP14 itself nor its mutant could block ChIP activity, while, when both BAG2 and NLRP14 were overexpressed, a significant decrease of HSPA2 ubiquitination was detected (Fig. 5*H*). Together, these data suggested that formation of the NLRP14–BAG2–HSPA2 complex was critical to maintain the homeostasis of HSPA2 and protect it from proteasomal degradation in the SSC line.

NLRP14 Promoted Nuclear Translocation of HSPA2. To investigate the functional consequence of HSPA2 stabilization by NLRP14-mediated

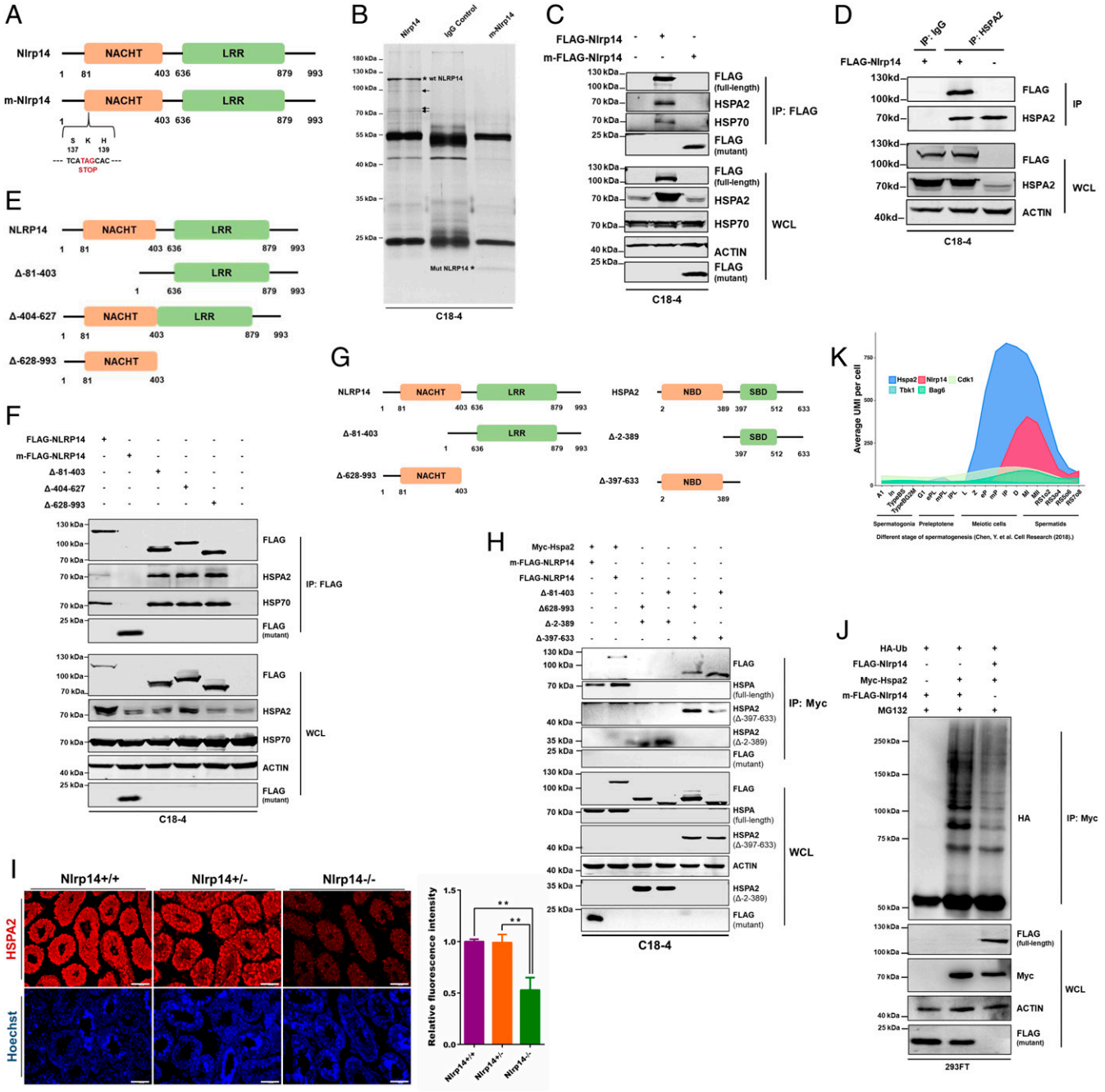

Fig. 4. NLRP14 interacted with HSPA2 and protected it from polyubiquitination in the SSC line. (*A*) Schematic of cloning strategy for WT and mutant mouse Nlrp14 for IP and mass spectrometry analysis. A STOP codon was introduced in K138 of NLRP14 to generate a truncated protein while maintaining the overall vector size. (*B*) Several proteins appeared to be specifically associated with NLRP14. IP of WT and mutant Nlrp14 was performed in C18-4 cells (immortalized mouse SSC line). A representative image of silver staining is shown. (*C*) Interaction between NLRP14, HSP70, and HSPA2 was confirmed by IP. FLAG-tagged mouse WT and mutant NLRP14 were expressed in C18-4 cells for 48 h and before co-IP and Western blot analysis for HSP70 and HSPA2. WCL, whole-cell lysate. (*D*) Reverse IP further confirmed the binding of HSPA2 with NLRP14. The experimental procedure was the same as in *C*. FLAG, full-length NLRP14 with FLAG tag. (*E*) Schematic of mouse NLRP14 truncation mutants. (*F*) Both the N-terminal NACHT domain and the LRR domain of mouse NLRP14 could bind to HSPA2 and HSP70. C18-4 cells were transfected with various combinations of vectors for 48 h before IP analysis. The expression of transgenes was first confirmed by anti-FLAG antibody and Western blotting. (*G*) Schematic of mouse NLRP14 and HSPA2 truncation mutants. (*H*) NBD domain of HSPA2 interacted with both NACHT and LRR domains of NLRP14. Myc-tagged full length and mutants of HSPA2 were coexpressed with NLRP14 in C18-4 cells for 48 h before co-IP. The expression of each mutant was first confirmed by Western blotting in WCL using the anti-Myc antibody. The expression of NLRP14 was analyzed by anti-FLAG Western blotting. (*I*) HSPA2 expression was significantly decreased in the testis of Nlrp14 KO mice. Immunofluorescence on testis sections from WT, heterozygous, and KO mice was performed. Relative fluorescence intensity per area was analyzed by ImageJ software and normalized with WT signal. For each section, five to six seminiferous tubules were analyzed. Error bar represents data from sections of three animals for each genotype. Statistics: one-way ANOVA followed by Tukey post hoc multiple comparisons (by SPSS). $^{**}P < 0.01$. Scale bar, 100 μm. (*J*) Interaction with NLRP14 protected HSPA2 from polyubiquitination. FLAG-tagged WT and mutant NLRP14 were coexpressed with Myc-HSPA2 and HA-Ub in 293FT cells for 48 h. IP with anti-HSPA2 antibody was performed, and the polyubiquitination was analyzed by Western blotting using an anti-HA antibody. MG-132 was added at 42 h posttransfection (6 h before harvest) at 10-μM final concentration. (*K*) Expression of Nlrp14 and Hspa2 were closely associated throughout spermatogenesis. Single-cell RNA-seq results from a previously published paper (32) were reanalyzed. Expression of Tbk1 (a previously identified Nlrp14 interacting protein), Bag6, and Cdk1 (HSPA2 interacting proteins) were included as the control for comparison. All co-IP experiments were repeated at least twice.

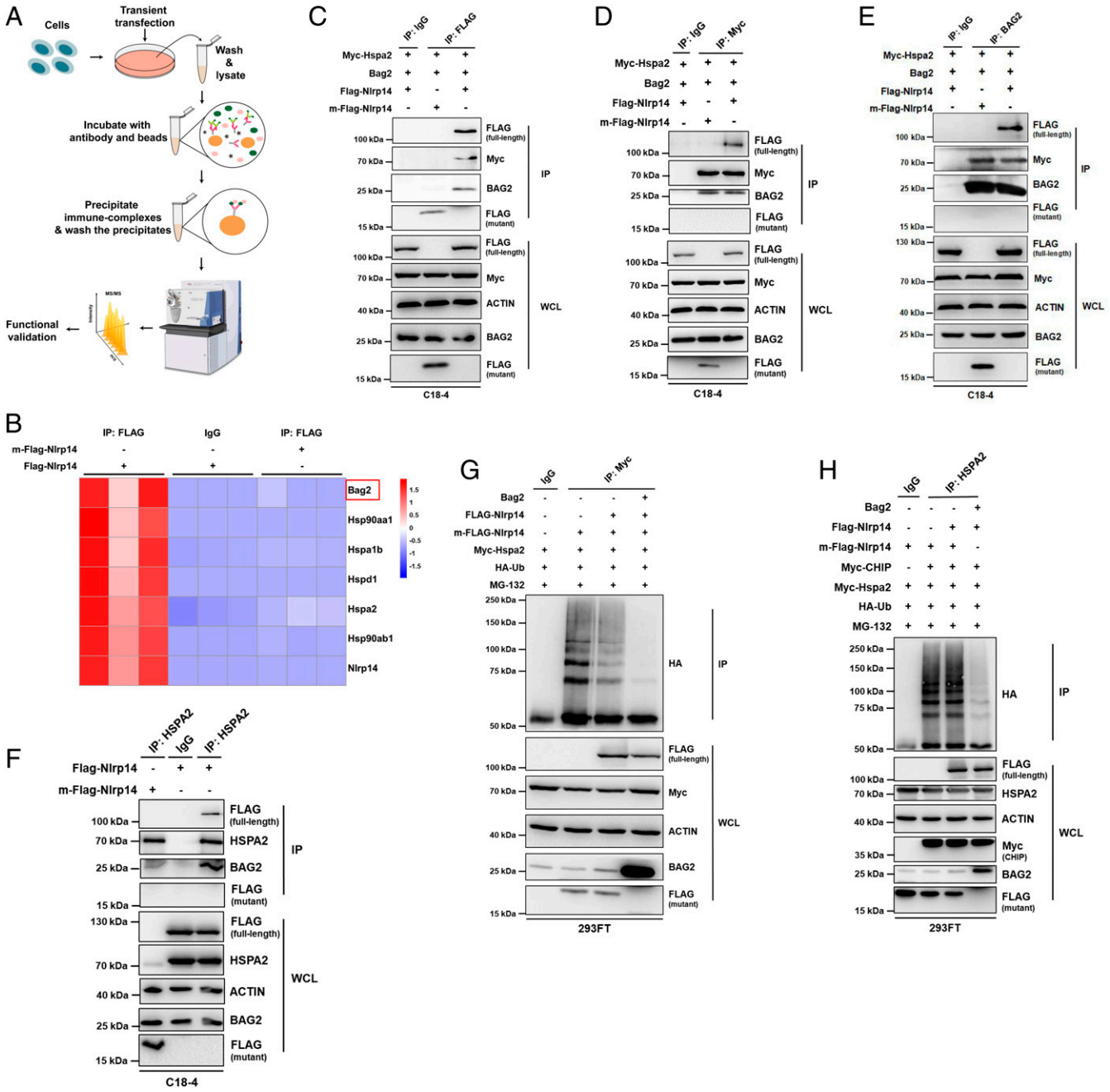

Fig. 5. NLRP14 inhibited HSPA2 ubiquitination through the recruitment of BAG2. (*A*) Schematic of IP-coupled mass spectrometry analysis for NLRP14 interacting proteins. (*B*) Seven proteins were specifically enriched in NLRP14-overexpressing C18-4 cells. The red box indicates BAG2. Full-length and mutant FLAG-tagged NLRP14 were expressed in C18-4 cells for 48 h before IP. IP samples from three independent experiments were used for mass spectrometry analysis. (*C*) IP by FLAG-NLRP14 confirmed the interaction among mouse NLRP14, HSPA2, and BAG2. Myc-HSPA2, BAG2, WT, and mutant FLAG-NLRP14 were coexpressed in C18-4 cells for 48 h before IP. (*D*) Reverse IP with Myc-HSPA2 also confirmed the interaction among mouse NLRP14, HSPA2, and BAG2. The experimental conditions were the same as in *C*. (*E*) Reverse IP with BAG2 also confirmed the interaction among mouse NLRP14, HSPA2, and BAG2. The experimental conditions were the same as in *C*. (*F*) Expression of mouse NLRP14 enhanced BAG2 IP by endogenous HSPA2. The experimental conditions were the same as in *C*. (*G*) NLRP14 and BAG2 strongly inhibited the polyubiquitination of HSPA2. The 293FT cells were cotransfected with different combinations of vectors for 48 h before IP analysis. Overexpression of respective genes was confirmed by Western blotting. MG-132 was added at 42 h posttransfection (6 h before harvest) at 10-μM final concentration. (*H*) NLRP14 and BAG2 inhibited ChIP-mediated polyubiquitination of HSPA2. The experimental conditions were the same as in *G*. All of the experiments in *C*–*H* were repeated at least twice.

protection, we focused on one of the key aspects of HSPA2's regulation on spermatogenesis: nuclear translocation to facilitate spermatid DNA packaging (18, 37). Both immunostaining (Fig. 6 *A* and *B*) and nuclear–cytoplasm protein fractionation (Fig. 6 *C*–*E*) supported that a substantial increase of HSPA2 translocation was detected in WT Nlrp14 cotransfected cells but not with mutant Nlrp14. In addition, the increase of HSPA2 in the nucleus was not merely due to an overall increased expression but also because of a higher percentage of HSPA2's translocation in the nucleus as the ratio between nuclear HSPA2 vs. the cytoplasmic one was increased (Fig. 6*F*). Altogether, our data suggested that NLRP14 might play a crucial role in regulating proteasomal

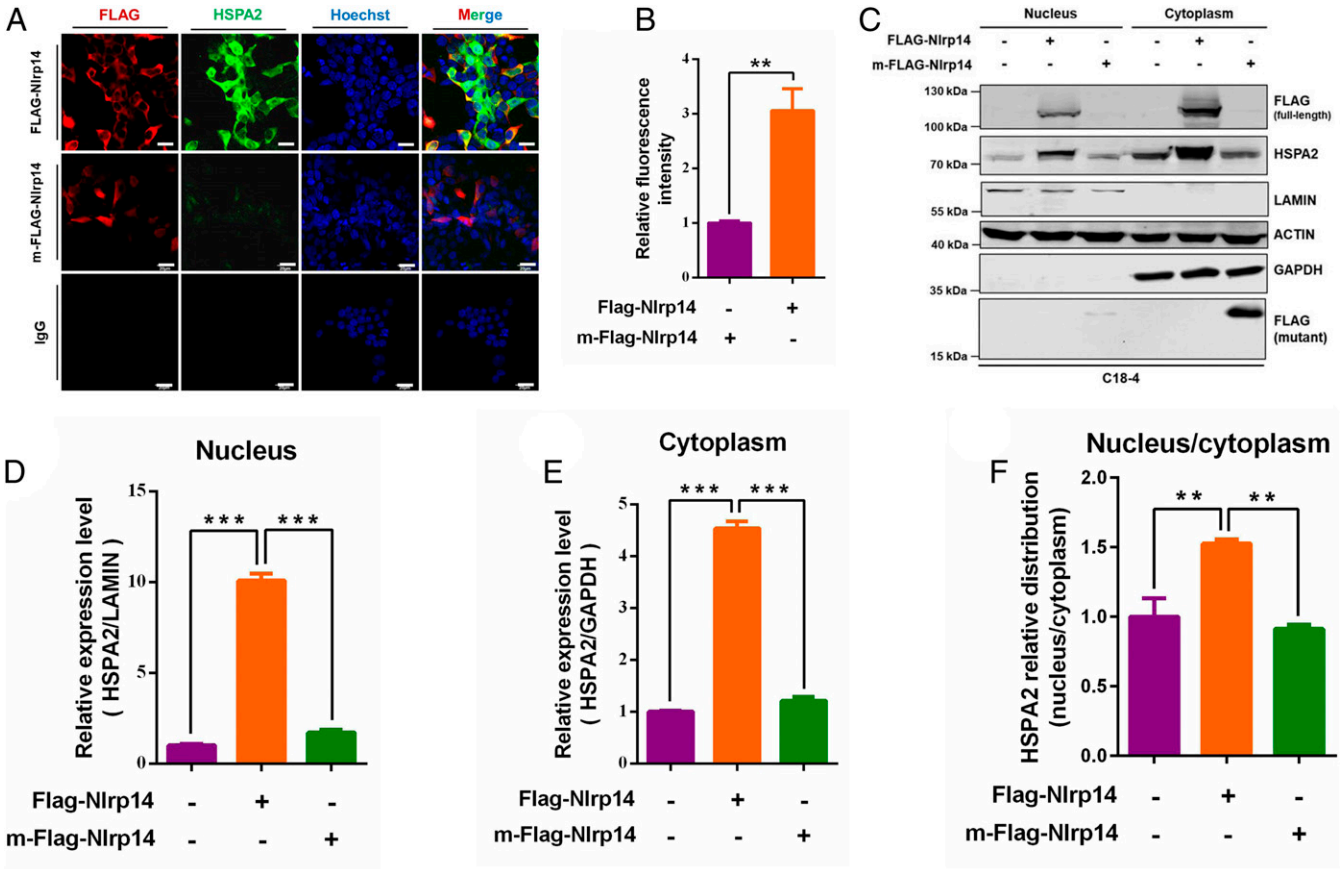

Fig. 6. NLRP14 promoted nuclear translocation of HSPA2. (*A*) NLRP14 enhanced HSPA2 expression in mouse C18-4 cells. Full-length and mutant mouse FLAG-tagged Nlrp14 were transfected into C18-4 cells for 24 h before immunostaining of endogenous HSPA2. HSPA2 signal was detected with anti-rabbit Alexa 488 secondary antibody. The expression of NLRP14 was confirmed by the anti-FLAG antibody. Hoechst was used for nuclear staining. (Scale bar: 20 μm.) (*B*) Quantitative analysis confirmed the increased HSPA2 expression in WT NLRP14-overexpressing C18-4 cells. HSPA2 fluorescence signal per area was measured by ImageJ software. Relative fluorescence intensity was calculated by normalizing to HSPA2 signal in mutant NLRP14 transfected cells. Error bar represents image signals from three independent experiments, three images per experimental group. Statistics: independent-sample *t* test (by SPSS). $^{**}P < 0.01$. (*C*) Overexpression of NLRP14 led to increased nuclear translocation of HSPA2. Full-length and mutant NLRP14 were transfected into C18-4 cells for 24 h before harvest for nucleus/cytoplasm fraction. The distribution of HSPA2 was measured by Western blotting. LAMIN and GAPDH were used as the nucleus and cytoplasmic markers, respectively. The experiment was repeated three times. Representative images are shown. (*D*) Quantitative analysis confirmed the increased expression of HSPA2 in the nucleus. Western blotting images were quantified by the LI-COR system and normalized to the LAMIN signal. Error bar represented data from three independent experiments. Statistics: one-way ANOVA followed by Tukey post hoc multiple comparisons (by SPSS). $^{***}P < 0.001$. (*E*) Quantitative analysis confirmed the increased expression of HSPA2 in the cytoplasm. The experimental conditions were the same as in *D*. $^{***}P < 0.001$. (*F*) The proportion of increased HSPA2 expression level in the nucleus was significantly higher in WT NLRP14 expressing cells than in mutant NLRP14 or the nontransfected control. Nuclear HSPA2 signal from each group was first normalized to nuclear Actin expression. Similar normalization was done for cytoplasmic HSPA2. The distribution ratio was calculated by normalized nuclear HSPA2/cytoplasmic HSPA2. All results were compared to nontransfected cells. Error bar represents data from three independent experiments. Statistics: one-way ANOVA followed by Tukey post hoc multiple comparisons (by SPSS). $^{**}P < 0.01$.

degradation of HSPA2, probably by recruitment of cochaperone proteins such as BAG2, which promoted nuclear translocation of HSPA2 to facilitate spermatid biogenesis.

The NLRP14–HSPA2–BAG2 Complex Was also Present in Human Cells. To test whether NLRP14–HSPA2–BAG2 interaction was also conserved in human samples, vectors expressing WT hNLRP14 and a nonsense germline variant associated with male sterility (STOP codon mutation at AA108) were constructed (Fig. 7*A*) (16). IP was performed in 293FT cells expressing these WT and mutant variants as well as HSPA2 and BAG2. The results confirmed that human NLRP14 would still interact with HSPA2 and BAG2, and vice versa, as these proteins could pull down each other in human cells (Fig. 7 *B*–*D*). In addition, we also confirmed that full-length NLRP14, together with BAG2, indeed also protected HSPA2 from polyubiquitination, while the nonsense mutant of NLRP14 could not (Fig. 7*E*). Together, these data supported that the interaction among NLRP14, HSPA2, and BAG2 was conserved among species, and it may be lost in a nonsense mutant of NLRP14 which is associated with human reproductivity failure.

Discussion

In this study, we analyzed the transcriptome data from ENCODE (14) to identify testis-specific genes. By cross-comparing with differential gene expression profiles from mESC–EpiLCs–PGCLCs, potential regulators of germ cell specification were identified. Through a targeted RNAi screen and KO animal study, an NLR Nlrp14 was found to be crucial for PGCLC specification, differentiation of SSCs, and meiosis. The further mechanistic study revealed that NLRP14 might function through forming a triple-protein complex with HSPA2 and BAG2, which protected HSPA2 from proteasome-mediated polyubiquitination and facilitated its nuclear translocation in SSCs. These data suggested a

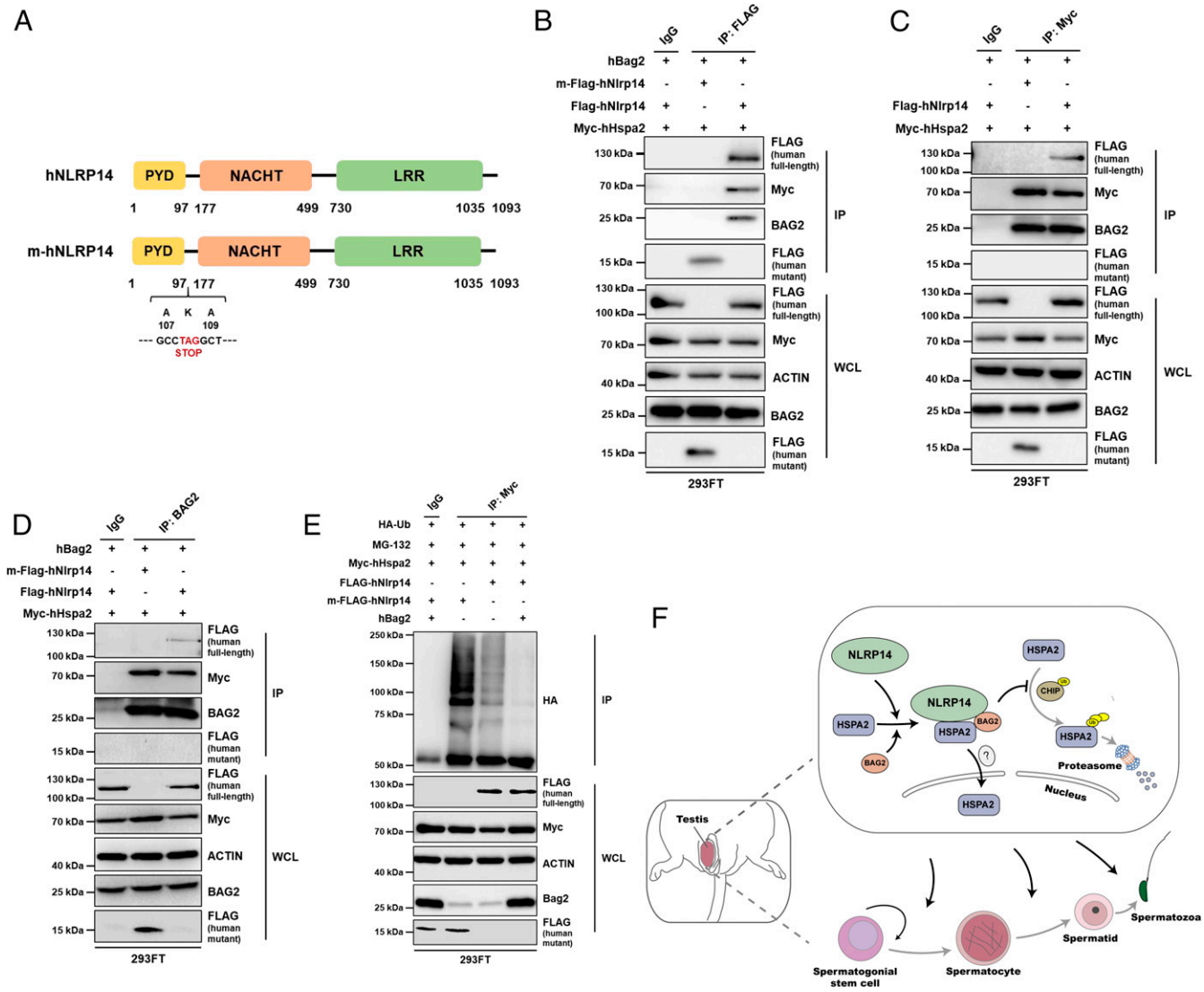

Fig. 7. NLRP14–HSPA2–BAG2 complex and its protection of HSPA2 from ubiquitination were also present in human cells. (*A*) Schematic of the cloning strategy for human WT and mutant Nlrp14. A STOP codon was introduced in K108 of human Nlrp14 to mimic a clinically relevant truncated mutant. (*B*) Co-IP confirmed the interaction among NLRP14, HSPA2, and BAG2 in human cells. Myc-HSPA2, BAG2, and WT or mutant NLRP14 were cotransfected in 293FT cells for 48 h before co-IP. Transgene expression was confirmed by Western blotting before IP. (*C* and *D*) Reverse IP with either HSPA2 or BAG2 antibody also confirmed the interaction among NLRP14, HSPA2, and BAG2. The experimental conditions were the same as in *B*. (*E*) The NLRP14-HSPA2-BAG2 complex protected HSPA2 from polyubiquitination in human cells. The 293FT cells were cotransfected with different combinations of vectors for 48 h before IP analysis. Overexpression of respective genes was confirmed by Western blotting. MG-132 was added at 42 h posttransfection (6 h before harvest) at 10-μM final concentration. (*F*) Model for the NLRP14–HSPA2–BAG2 complex-mediated regulation on spermatogenesis in adult mice. All of the IP experiments were repeated at least twice.

critical role for the NLRP14–HSPA2–BAG2 complex in germ cell specification and spermatogenesis (Fig. 7*F*). Unlike its other family members, few reports are currently available for Nlrp14's function, although it was long known to have specific expressions in testis and ovary. Our study provides evidence on the physiological function of Nlrp14 in regulating germ cell development. Nlrp14 is also the only reported member in the NLR family that plays a critical role in both female and male reproductivity.

Over a decade after the first discovery that identified Nlrp14 mutations were associated with male spermatogenic failure (16), a recent report emphasized its role in inhibiting cytosolic nucleic acid-sensing machinery through degradation of Tbk1 kinase and potentially promoting fertilization (15). Tbk1 has been reported to have multiple roles in innate immunity (38), autophagy (39, 40), neuroinflammation (41), and amyotrophic lateral sclerosis (42). The function of Tbk1 was closely linked with RIPK1, where Tbk1 KO embryonic lethality could be fully rescued by transgenic expression of RIPK1 dominant-negative mutant, and, at the same time, Tbk1 also showed inhibitory effects on RIPK1-independent apoptosis induced by TNF-α/cycloheximide (43). Moreover, the RIPK1/RIPK3 complex promotes aging in the male reproductive system in mice but is not required for germ cell development (44). In this regard, Tbk1 is unlikely to be the main downstream partner of Nlrp14 in germ cell specification and spermatogenesis. Indeed, in our study, NLRP14 was found to form a protein complex with HSPA2 instead of TBK1 to regulate PGCLC differentiation and spermatogenesis. HSPA2 is an indispensable gene for male germ cell development, deficiency of which caused trapped spermatogenic cell development, disrupted meiosis, and the apoptotic elimination of late-stage pachytene spermatocytes (30, 33). The phenotypes detected in our Nlrp14 KO animals were indeed consistent with these observations. Additionally, in

our experiments, we found that NLRP14's interaction with HSPA2 enhanced its nuclear translocation, which matched with the earlier findings that HSPA2 could facilitate translocation of the major spermatid DNA packaging proteins TP1 and TP2 into the nucleus (18), and decreased HSPA2 expression was associated with immature and abnormal sperms that had been adopted in clinical use in men (45, 46), which were also observed in sperms from NLRP14-deficient mice. Moreover, a close correlation of Nlrp14 and Hspa2 was also found in the same group of cells from reanalyzing previous single-cell transcriptome datasets, which supported the claim that the NLRP14–HSPA2 complex played a pivotal role in germ cell development and spermatogenesis.

The finding that NLRP14 protected HSPA2 from ChIP-mediated polyubiquitination and proteasomal degradation by forming the NLRP14–HSPA2–BAG2 complex provides an intriguing point for the physiological function of NLR family genes. Canonically, NLR family genes, which include four subfamilies (NLRA, NLRB, NLRC, and NLRP) depending on their N-terminal effector domains (47), are believed to act as a class of PRRs in inflammasome-mediated responses (6). Most of the NLRP subfamily are indeed documented with such activities, including Nlrp1 (48), Nlrp2 (49), Nlrp3 (50), Nlrp6 (51), and Nlrp9 (52). However, there are outliers as well. For example, Nlrp4 and Nlrp11 seem to suppress IFN- or TLR-mediated immune responses by ubiquitination and proteasomal degradation, not through the inflammasomes (53, 54). Although these reports support that many NLRPs did function through immune-related pathways, the situation for gonad-specific NLRPs seems to be different. There are four gonad-specific NLRPs in mice and human: NLRP2, NLRP5, NLRP7, and NLRP14. NLRP7 does not have an ortholog in mice, while NLRP2 and NLRP5 are the most studied ones. NLRP2 selectively regulates early embryonic development and age-associated fertility but is not involved in any innate or adaptive immune responses (10). NLRP5, a maternal gene expressed only in oocytes, is again required for early embryonic development of fertilized egg, but its deficiency does not lead to any immune-related abnormalities in mice (11). However, the molecular mechanisms of NLRP2- and NLRP5-mediated maternal effects are not reported yet. For NLRP14, it was found to suppress nucleic acid-sensing immune responses through inhibiting TBK1-mediated pathways in 293T cells and proposed to act similarly in fertilized egg (15), but the physiological function was not known to date. Therefore, our study provides a valuable piece of information that NLRP14 plays a pivotal role in regulating PGCLC differentiation and spermatogenesis through forming a complex with HSPA2 and BAG2. This interaction results in protection of HSPA2 from proteasomal degradation and facilitates its translocation in nucleus. These findings not only offer functional insights on NLRP14's long overdue physiological function but also suggest that proteasome-associated functions, rather than immune regulations, could be the general mechanism of action for gonad-specific NLRPs

Nevertheless, it is worth noting that there are a few remaining questions that warrant further investigation. One such is regarding the role of NLRP14 in PGC development in vivo. Although PGCLC differentiation has been used widely as a surrogate assay to investigate PGC development (55–57), to knock out NLRP14 in the fluorescence-labeled primary PGC transgenic animal models will be informative to see whether NLRP14 has a role in germ cell development in vivo. Secondly, the C18-4 cells used in our study were an immortalized SSC line (29) which were characterized with typical SSC marker expression (*SI Appendix*, Fig. S7 *A* and *B*) (58) and had been extensively used for investigating self-renewal regulation of SSCs (59–61) and in vitro germline toxicity assessment (62); however, their competence for continued spermatogenesis was not proven. While other germline stem cells, such as mouse GS cells (63), would be a closer mimic of primary SSCs, the transgene delivery method (mainly through electroporation) and its relatively low efficiency limited large-scale biochemical analysis of them (64–66). Therefore, it will be also important to confirm whether the triple complex could be detected in primary SSCs by using transgenic mouse models. In addition, the increased expression and cleavage of caspases suggested that apoptosis might be one of the leading routes taken by SSCs trapped in the undifferentiated state. However, whether other cell death pathways (necrosis, pyroptosis, etc.) may contribute to the Nlrp14 KO defects requires further investigation. Finally, the role of Nlrp14 in female reproduction remain to be solved, because HSPA2 KO females remained fertile and thus HSPA2 was unlikely to contribute to the phenotype observed in Nlrp14 KO female animals (30). It will be interesting to elaborate on whether proteasome-mediated regulation would again stand out in these studies.

Materials and Methods

Generation of the Nlrp14 KO ES Cell Line. All animal protocols are approved by the Animal Care and Use Committee of the Model Animal Research Center, College of Life Sciences, Sichuan University. AB2.2 mESCs were used to generate the Nlrp14 KO cell line using the CRISPR-Cas9 method. Two single guide RNAs (sgRNAs) targeting the third and fifth exon of mouse Nlrp14 were designed by using an online tool (http://tools.genome-engineering.org). The sgRNA sequences are listed in *SI Appendix*, Table S2. The sgRNA oligos were annealed and cloned into pX330 backbone. The pX330-Cas9-sgNlrp14s were then transfected into AB2.2 mES cells using Lipofectamine 3000 (L3000-015, Invitrogen). Forty-eight hours after transfection, cells were seeded in 96-well gelatin-coated plates at a concentration of 0.5 cells per well, and single colonies were derived within 5 d to 7 d later. Genomic DNAs from different colonies were extracted and analyzed by PCR. Each amplified fragment was also confirmed by Sanger sequencing. Primers sequences are listed in *SI Appendix*, Table S3 as Nlrp14 primer sets 1 to 3.

Data Availability. All study data are included in the article and *SI Appendix*.

ACKNOWLEDGMENTS. We thank Han Kang from Core Facilities in College of Life Sciences and Yufeng Duan from National Engineering Laboratory for Oral Regenerative Medicine for their technical assistance. We thank Prof. Yuan Wang from East China Normal University for her generous gift of C18-4 cells. We thank Prof. Wei Li from Institute of Zoology, Chinese Academy of Sciences, for his insightful discussion and suggestions on the manuscript. This work was supported by National Key Research and Development Program of China (Grant 2017YFA0104801), National Natural Science Foundation of China (Grants 31900900 and 31401262), China Postdoctoral Science Foundation (Grant 2018M633361), Postdoctoral Fellowship of Sichuan University (Grant 2018SCU12053), "One Thousand Talents" program from the Chinese Central Government and Sichuan Province, and the Fundamental Research Funds for the Central Universities (Grant SCU2019D013).

1. S. W. Brubaker, K. S. Bonham, I. Zanoni, J. C. Kagan, Innate immune pattern recognition: A cell biological perspective. *Annu. Rev. Immunol.* **33**, 257–290 (2015).
2. G. Chen, M. H. Shaw, Y. G. Kim, G. Nuñez, NOD-like receptors: Role in innate immunity and inflammatory disease. *Annu. Rev. Pathol.* **4**, 365–398 (2009).
3. Y. M. Loo, M. Gale Jr., Immune signaling by RIG-I-like receptors. *Immunity* **34**, 680–692 (2011).
4. H. Wen, E. A. Miao, J. P. Ting, Mechanisms of NOD-like receptor-associated inflammasome activation. *Immunity* **39**, 432–441 (2013).
5. C. Lupfer, T. D. Kanneganti, The expanding role of NLRs in antiviral immunity. *Immunol. Rev.* **255**, 13–24 (2013).
6. P. Broz, V. M. Dixit, Inflammasomes: Mechanism of assembly, regulation and signalling. *Nat. Rev. Immunol.* **16**, 407–420 (2016).
7. T. B. Meissner *et al.*, NLR family member NLRC5 is a transcriptional regulator of MHC class I genes. *Proc. Natl. Acad. Sci. U.S.A.* **107**, 13794–13799 (2010).
8. J. K. Krishnaswamy, T. Chu, S. C. Eisenbarth, Beyond pattern recognition: NOD-like receptors in dendritic cells. *Trends Immunol.* **34**, 224–233 (2013).
9. H. Peng *et al.*, Nlrp2, a maternal effect gene required for early embryonic development in the mouse. *PLoS One* **7**, e30344 (2012).
10. A. A. Kuchmiy, J. D'Hont, T. Hochepied, M. Lamkanfi, NLRP2 controls age-associated maternal fertility. *J. Exp. Med.* **213**, 2851–2860 (2016).
11. Z. B. Tong *et al.*, Mater, a maternal effect gene required for early embryonic development in mice. *Nat. Genet.* **26**, 267–268 (2000).
12. S. Murdoch *et al.*, Mutations in NALP7 cause recurrent hydatidiform moles and reproductive wastage in humans. *Nat. Genet.* **38**, 300–302 (2006).
13. E. Akoury, L. Zhang, A. Ao, R. Slim, NLRP7 and KHDC3L, the two maternal-effect proteins responsible for recurrent hydatidiform moles, co-localize to the oocyte cytoskeleton. *Hum. Reprod.* **30**, 159–169 (2015).

14. C. A. Davis *et al*., The encyclopedia of DNA elements (ENCODE): Data portal update. *Nucleic Acids Res.* **46**, D794–D801 (2018).
15. T. Abe *et al*., Germ-cell-specific inflammasome component NLRP14 negatively regulates cytosolic nucleic acid sensing to promote fertilization. *Immunity* **46**, 621–634 (2017).
16. G. H. Westerveld *et al*., Mutations in the testis-specific NALP14 gene in men suffering from spermatogenic failure. *Hum. Reprod.* **21**, 3178–3184 (2006).
17. B. Nixon, E. G. Bromfield, J. Cui, G. N. De Iuliis, Heat shock protein A2 (HSPA2): Regulatory roles in germ cell development and sperm function. *Adv. Anat. Embryol. Cell Biol.* **222**, 67–93 (2017).
18. J. Govin *et al*., Post-meiotic shifts in HSPA2/HSP70.2 chaperone activity during mouse spermatogenesis. *J. Biol. Chem.* **281**, 37888–37892 (2006).
19. V. Arndt, C. Daniel, W. Nastainczyk, S. Alberti, J. Höhfeld, BAG-2 acts as an inhibitor of the chaperone-associated ubiquitin ligase CHIP. *Mol. Biol. Cell* **16**, 5891–5900 (2005).
20. K. Hayashi, H. Ohta, K. Kurimoto, S. Aramaki, M. Saitou, Reconstitution of the mouse germ cell specification pathway in culture by pluripotent stem cells. *Cell* **146**, 519–532 (2011).
21. S. L. Byers, S. J. Payson, R. A. Taft, Performance of ten inbred mouse strains following assisted reproductive technologies (ARTs). *Theriogenology* **65**, 1716–1726 (2006).
22. P. Quinn, J. F. Kerin, G. M. Warnes, Improved pregnancy rate in human in vitro fertilization with the use of a medium based on the composition of human tubal fluid. *Fertil. Steril.* **44**, 493–498 (1985).
23. M. Saitou, H. Miyauchi, Gametogenesis from pluripotent stem cells. *Cell Stem Cell* **18**, 721–735 (2016).
24. T. L. Beumer, H. L. Roepers-Gajadien, I. S. Gademan, H. B. Kal, D. G. de Rooij, Involvement of the D-type cyclins in germ cell proliferation and differentiation in the mouse. *Biol. Reprod.* **63**, 1893–1898 (2000).
25. L. Yuan *et al*., The murine SCP3 gene is required for synaptonemal complex assembly, chromosome synapsis, and male fertility. *Mol. Cell* **5**, 73–83 (2000).
26. W. Gu *et al*., Mammalian male and female germ cells express a germ cell-specific Y-Box protein, MSY2. *Biol. Reprod.* **59**, 1266–1274 (1998).
27. J. R. Hagaman *et al*., Angiotensin-converting enzyme and male fertility. *Proc. Natl. Acad. Sci. U.S.A.* **95**, 2552–2557 (1998).
28. S. Morais da Silva *et al*., Sox9 expression during gonadal development implies a conserved role for the gene in testis differentiation in mammals and birds. *Nat. Genet.* **14**, 62–68 (1996).
29. M. C. Hofmann, L. Braydich-Stolle, L. Dettin, E. Johnson, M. Dym, Immortalization of mouse germ line stem cells. *Stem Cells* **23**, 200–210 (2005).
30. D. J. Dix *et al*., Targeted gene disruption of Hsp70-2 results in failed meiosis, germ cell apoptosis, and male infertility. *Proc. Natl. Acad. Sci. U.S.A.* **93**, 3264–3268 (1996).
31. T. Sasaki *et al*., Bat3 deficiency accelerates the degradation of Hsp70-2/HspA2 during spermatogenesis. *J. Cell Biol.* **182**, 449–458 (2008).
32. Y. Chen *et al*., Single-cell RNA-seq uncovers dynamic processes and critical regulators in mouse spermatogenesis. *Cell Res.* **28**, 879–896 (2018).
33. D. Zhu, D. J. Dix, E. M. Eddy, HSP70-2 is required for CDC2 kinase activity in meiosis I of mouse spermatocytes. *Development* **124**, 3007–3014 (1997).
34. Q. Dai *et al*., Regulation of the cytoplasmic quality control protein degradation pathway by BAG2. *J. Biol. Chem.* **280**, 38673–38681 (2005).
35. C. Rogon *et al*., HSP70-binding protein HSPBP1 regulates chaperone expression at a posttranslational level and is essential for spermatogenesis. *Mol. Biol. Cell* **25**, 2260–2271 (2014).
36. R. Rosenzweig, N. B. Nillegoda, M. P. Mayer, B. Bukau, The Hsp70 chaperone network. *Nat. Rev. Mol. Cell Biol.* **20**, 665–680 (2019).
37. J. Liu, J. Xia, K. H. Cho, D. E. Clapham, D. Ren, CatSperbeta, a novel transmembrane protein in the CatSper channel complex. *J. Biol. Chem.* **282**, 18945–18952 (2007).
38. K. A. Fitzgerald *et al*., IKKepsilon and TBK1 are essential components of the IRF3 signaling pathway. *Nat. Immunol.* **4**, 491–496 (2003).
39. T. L. Thurston, G. Ryzhakov, S. Bloor, N. von Muhlinen, F. Randow, The TBK1 adaptor and autophagy receptor NDP52 restricts the proliferation of ubiquitin-coated bacteria. *Nat. Immunol.* **10**, 1215–1221 (2009).
40. M. Pilli *et al*., TBK-1 promotes autophagy-mediated antimicrobial defense by controlling autophagosome maturation. *Immunity* **37**, 223–234 (2012).
41. L. Ahmad, S. Y. Zhang, J. L. Casanova, V. Sancho-Shimizu, Human TBK1: A gatekeeper of neuroinflammation. *Trends Mol. Med.* **22**, 511–527 (2016).
42. J. A. Oakes, M. C. Davies, M. O. Collins, TBK1: A new player in ALS linking autophagy and neuroinflammation. *Mol. Brain* **10**, 5 (2017).
43. D. Xu *et al*., TBK1 suppresses RIPK1-driven apoptosis and inflammation during development and in aging. *Cell* **174**, 1477–1491.e19 (2018).
44. D. Li *et al*., RIPK1-RIPK3-MLKL-dependent necrosis promotes the aging of mouse male reproductive system. *eLife* **6**, e27692 (2017).
45. G. Huszar, K. Stone, D. Dix, L. Vigue, Putative creatine kinase M-isoform in human sperm is identifiedas the 70-kilodalton heat shock protein HspA2. *Biol. Reprod.* **63**, 925–932 (2000).
46. S. Cayli *et al*., Biochemical markers of sperm function: Male fertility and sperm selection for ICSI. *Reprod. Biomed. Online* **7**, 462–468 (2003).
47. J. P. Ting *et al*., The NLR gene family: A standard nomenclature. *Immunity* **28**, 285–287 (2008).
48. S. L. Masters *et al*., NLRP1 inflammasome activation induces pyroptosis of hematopoietic progenitor cells. *Immunity* **37**, 1009–1023 (2012).
49. J. Minkiewicz, J. P. de Rivero Vaccari, R. W. Keane, Human astrocytes express a novel NLRP2 inflammasome. *Glia* **61**, 1113–1121 (2013).
50. K. Schroder, R. Zhou, J. Tschopp, The NLRP3 inflammasome: A sensor for metabolic danger? *Science* **327**, 296–300 (2010).
51. E. Elinav *et al*., NLRP6 inflammasome regulates colonic microbial ecology and risk for colitis. *Cell* **145**, 745–757 (2011).
52. S. Zhu *et al*., Nlrp9b inflammasome restricts rotavirus infection in intestinal epithelial cells. *Nature* **546**, 667–670 (2017).
53. J. Cui *et al*., NLRP4 negatively regulates type I interferon signaling by targeting the kinase TBK1 for degradation via the ubiquitin ligase DTX4. *Nat. Immunol.* **13**, 387–395 (2012).
54. C. Wu *et al*., NLRP11 attenuates Toll-like receptor signalling by targeting TRAF6 for degradation via the ubiquitin ligase RNF19A. *Nat. Commun.* **8**, 1977 (2017).
55. F. Nakaki *et al*., Induction of mouse germ-cell fate by transcription factors in vitro. *Nature* **501**, 222–226 (2013).
56. N. Irie *et al*., SOX17 is a critical specifier of human primordial germ cell fate. *Cell* **160**, 253–268 (2015).
57. S. Aramaki *et al*., A mesodermal factor, T, specifies mouse germ cell fate by directly activating germline determinants. *Dev. Cell* **27**, 516–529 (2013).
58. Z. He *et al*., Gdnf upregulates c-Fos transcription via the Ras/Erk1/2 pathway to promote mouse spermatogonial stem cell proliferation. *Stem Cells* **26**, 266–278 (2008).
59. Z. He, J. Jiang, M. Kokkinaki, M. Dym, Nodal signaling via an autocrine pathway promotes proliferation of mouse spermatogonial stem/progenitor cells through Smad2/3 and Oct-4 activation. *Stem Cells* **27**, 2580–2590 (2009).
60. L. Braydich-Stolle, N. Kostereva, M. Dym, M. C. Hofmann, Role of Src family kinases and N-Myc in spermatogonial stem cell proliferation. *Dev. Biol.* **304**, 34–45 (2007).
61. Z. Du *et al*., Melatonin attenuates detrimental effects of diabetes on the niche of mouse spermatogonial stem cells by maintaining Leydig cells. *Cell Death Dis.* **9**, 968 (2018).
62. L. Braydich-Stolle, S. Hussain, J. J. Schlager, M. C. Hofmann, In vitro cytotoxicity of nanoparticles in mammalian germline stem cells. *Toxicol. Sci.* **88**, 412–419 (2005).
63. M. Kanatsu-Shinohara *et al*., Long-term proliferation in culture and germline transmission of mouse male germline stem cells. *Biol. Reprod.* **69**, 612–616 (2003).
64. K. M. Chapman *et al*., Targeted germline modifications in rats using CRISPR/Cas9 and spermatogonial stem cells. *Cell Rep.* **10**, 1828–1835 (2015).
65. Y. Wu *et al*., Correction of a genetic disease by CRISPR-Cas9-mediated gene editing in mouse spermatogonial stem cells. *Cell Res.* **25**, 67–79 (2015).
66. T. Shinohara *et al*., Transfer of a mouse artificial chromosome into spermatogonial stem cells generates transchromosomic mice. *Stem Cell Reports* **9**, 1180–1191 (2017).